

# Spatially resolved photoresponse measurements on pentacene thin-film transistors

M. Fiebig · C. Erlen · M. Göllner · P. Lugli · B. Nickel

Received: 28 July 2008 / Accepted: 24 November 2008 / Published online: 17 December 2008  
© Springer-Verlag 2008

**Abstract** A confocal setup with a spatial resolution in the submicron regime is employed for investigating the response of pentacene transistors to local illumination. The transistors show enhanced and inhomogeneous photoresponse in the proximity of the hole-injecting contact. These inhomogeneities represent contact areas of varying injection efficiency. Thus, this technique allows imaging of contact efficiencies with submicron resolution over large areas up to hundreds of microns. Drift–diffusion simulations including a photogeneration/recombination process have been performed to model the photoresponse. The simulations illustrate that the potential drop along the channel is dramatically reduced in the illuminated area due to photoconductance (i.e. photoinjection of excitons and subsequent dissociation). Also, the injection barrier for holes is reduced if the illumination is close to the hole-injecting electrode. The rapid decay of the photoresponse with increasing distance to the positively biased electrode is caused by the limited electron mean free path in our devices.

PACS 73.40.Cg · 73.50.Gr · 73.50.Pz · 73.61.Ph · 73.61.-r

## 1 Introduction

Performance of organic thin-film transistors (OTFTs) has witnessed continuous improvement over the past years and has reached a level at which devices become suited for widespread application [1–3]. Nevertheless, the understanding of electronic transport and limiting factors of these devices is less developed compared to standard MOSFET technology. In this context, organic semiconductor/metal contacts [4–7] turned out to be a bottleneck for the performance of organic TFTs. Thus, their improvement [8–10] has experienced great attention. So far, methods for investigating contact qualities have mainly been four-terminal measurements [4, 5] and measurements at samples with different channel lengths [6, 7]. In this work we have implemented a modified spatially resolved photoresponse technique [11] for the study of bottom-contact pentacene TFTs (see Fig. 1). We demonstrate that this technique enables us to visualize contact deficiencies. We have also analyzed the experimental results using a drift–diffusion simulation, which allows us to estimate the carrier-injection barrier and recombination rates of photogenerated charge carriers.

## 2 Experimental methods

In the experimental setup, a He–Ne laser with 633-nm wavelength is used, which is in a regime of high absorption [12] and high quantum efficiency for pentacene [13]. After passing a chopper, lenses, beam splitters, and glass fibers, the light is focused by a confocal microscope at the sample surface to a diffraction-limited lateral spot size of approx. 0.5 μm at a total power of 10 μW. The sample was placed atop of a piezo-driven stage consisting of three positioning modules for all spatial dimensions. The modules work

M. Fiebig · M. Göllner · B. Nickel (✉)  
Department für Physik and CeNS,  
Ludwig-Maximilians-Universität, Geschwister-Scholl-Platz 1,  
80539, München, Germany  
e-mail: [nickel@lmu.de](mailto:nickel@lmu.de)

C. Erlen · P. Lugli  
Institute for Nanoelectronics, Technische Universität München,  
Arcisstrasse 21, 80333, München, Germany

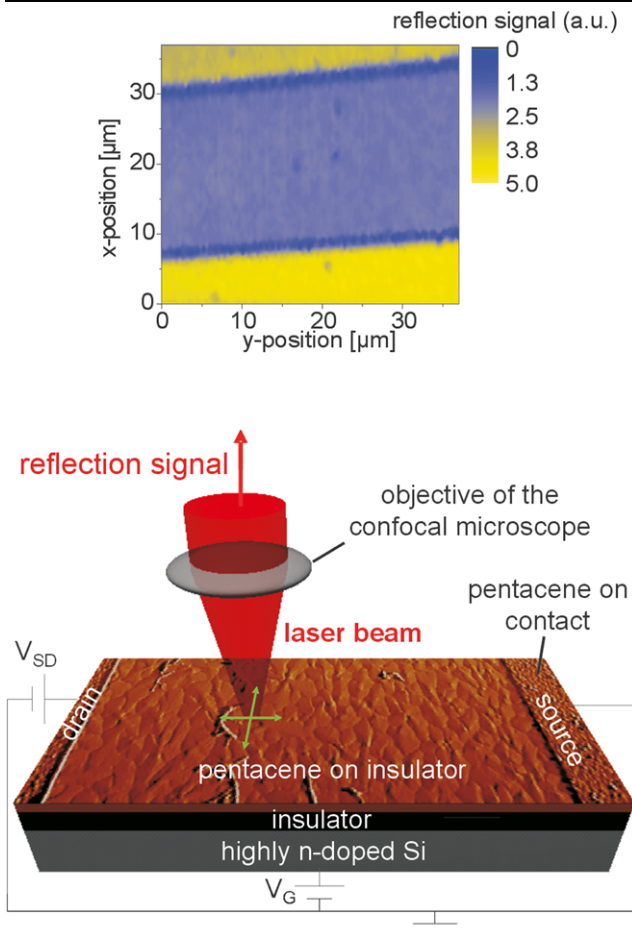


**Fig. 1** Schematic illustration of the spatially resolved photoresponse setup. The photoresponse of the source–drain current is measured by lock-in techniques while the focused laser is scanned across the transistor channel. Simultaneously, the reflected laser light is measured confocally in order to image the channel optically, which allows us to identify the contact positions (see *top* of the figure)

by the slip and stick principle [14] allowing us to scan an area of several micrometers with submicron resolution. In order to preposition the laser spot in the channel region, we defocused the light to identify the electrodes using the reflection signal. After refocusing the beam, the whole transistor channel is scanned under different gate and source–drain bias conditions. Sample reflectivity, indicating the exact position of our electrodes, and drain-current photoresponse were measured under ambient conditions simultaneously. The signals were extracted using a lock-in technique with a chopper frequency of about 1 kHz. The measured photoresponse characteristic therefore originates from physical processes that are at least faster than the chopper time scale, which is 1 ms. Hence, the influence of slow processes such as long-term charging effects (compare [11]) or persistent photocurrent is suppressed.

Bottom-contact pentacene TFTs were fabricated on a highly *n*-doped silicon substrate functioning as back gate

(see inset in Fig. 2a). A 150-nm layer of thermally grown  $\text{SiO}_2$  served as gate dielectric. Additionally a 3–6 nm-thick buffer layer of either cyclic olefin copolymer or polystyrene was spin coated on top of the silicon oxide. Source and drain contacts consisting of 3-nm Ti for adhesion and 30-nm to 60-nm Au were defined using a shadow mask. Finally, a 20-nm- to 50-nm-thick layer of purified pentacene was deposited at room temperature, at a pressure of about  $10^{-8}$  mbar and at a rate of about 0.1 Å/s, so that we obtained completely covering films [15]. The channel length and widths of our samples were 25 and 1000 to 4000 μm, respectively.

### 3 Results

These devices exhibited, if exposed to air, mobilities of up to  $0.1 \text{ cm}^2 \text{ V}^{-1} \text{s}^{-1}$ , subthreshold slopes down to 1 V/decade, and on/off ratios of up to  $10^6$ . Transport characteristics under ambient conditions of a sample with a buffer layer of polystyrene are shown in Fig. 2.

A photoresponse map of a transistor region showing 250 μm of the channel is shown in Fig. 3a. The plotted intensities represent the photoresponse as a function of the *x*–*y* position of the laser spot on the surface. The map was stitched together from several scans which could be aligned precisely using the reflection maps. The small differences at the stitching edges can be explained by different bias stresses that the sample was exposed to for the different scans. As the transport curves of our transistors show hysteresis (compare Fig. 2a), we assign this to a different amount of activated trapped states that influence the photoresponse signal. Besides these small discontinuities, two major qualitative features can be observed. First, the photoresponse is highly inhomogeneous along the source contact; the maximum photoresponse varies between 1 and 3.5 nA. We assign this inhomogeneous behavior to the varying quality of the pentacene film near the contacts [16]. Typical atomic force microscopy images of the transistors (compare Fig. 1) confirm that near the contacts the average pentacene grain size decreases. Second, the photoresponse is strongly enhanced at the positively biased electrode. To further confirm this behavior, two photoresponse maps with exactly antisymmetric bias combinations are presented in Fig. 3b and c. In both cases the photoresponse signal is clearly increased close to the more positively biased electrode, which is the source in Fig. 3b and the drain in Fig. 3c.<sup>1</sup>

Altogether, we have measured the spatially resolved photoresponse at more than 10 devices with different buffer lay-

<sup>1</sup>The two measurement sets are obtained at antisymmetrical bias situations, as the gate source voltage of Fig. 3b is equal to the gate drain voltage of Fig. 3c and vice versa.

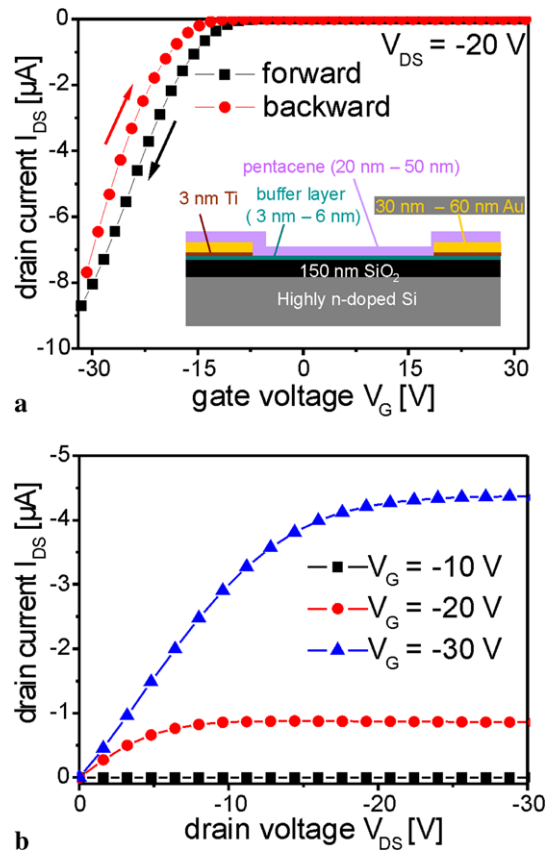


**Fig. 2** Transport characteristics for a pentacene TFT with a polystyrene buffer layer. (a)  $I_{DS}$  vs.  $V_G$  curves for a source–drain voltage of  $V_{DS} = -20$  V. Forward and backward sweeps are presented. The inset shows schematically the cross section of our samples. (b)  $I_{DS}$  vs.  $V_D$  curves for various gate voltages

ers from different samples applying various bias combinations. Besides the fabrication process described above, some of these samples were also produced using optical lithography for defining gold or palladium contacts. All of our samples showed qualitatively the described photoresponse behavior. Using light intensities up to  $30 \mu\text{W}$ , only a small but spatially uniform decrease of the photoresponse signal could be observed if the same area was scanned several tens of times.

#### 4 Discussion

A model describing the photoresponse increase towards the positively biased electrode is proposed in the following. We assume that the absorption of photons leads to photogenerated electrons and holes with a certain efficiency  $\eta$ . In turn, local illumination causes a gradient in the carrier densities, resulting in a diffusion of photogenerated electrons and holes into the surrounding region. A drift current that results from the applied source–drain field superimposes this diffusion process. Recombination processes consume the photo-

generated carriers while they move along the channel, limiting the number of charges and defining an equilibrium density in the illuminated region.

The photogeneration  $G_{hv}$  at the location of the laser spot is given by

$$G_{hv} = \eta \cdot \alpha \cdot \frac{P_{\text{opt}}}{h\nu}, \quad (1)$$

where  $P_{\text{opt}}$  is the optical power density,  $\alpha$  the absorption coefficient,  $\eta$  the efficiency of free-carrier generation, and  $h\nu$  the photon energy. For  $\lambda = 633 \text{ nm}$  we have measured a pentacene absorption of  $\alpha = 7.7 \times 10^4 \text{ cm}^{-1}$ . With respect to the recombination, we assume a bimolecular recombination rate  $R$  that is described by

$$R = r \cdot n(x) \cdot p(x), \quad (2)$$

where  $r$  is the recombination coefficient and  $n(x)$  ( $p(x)$ ) is the electron (hole) density in dependence on the distance  $x$  to the source contact.

Based on these assumptions, two different mechanisms both resulting in a photoresponse signal are possible. *Mechanism 1 (photocurrent)*: both photocarriers of a photogenerated electron and hole pair are extracted at the contacts and a photocurrent flows. *Mechanism 2 (photoconductance)*: even if both carriers are not extracted, the high density of photogenerated carriers increases the conductance of the organic semiconductor in the region of the laser spot, resulting in an increased current [17].

For mechanism 1 (photocurrent), it is essential that both electrodes are within reach of the photogenerated carriers. The electron mean free path (e-MFP) is limited by the recombination probability of the photogenerated electrons with both photogenerated holes and holes injected by the source contact. In contrast, the hole mean free path (h-MFP) is mainly limited by hole recombination with photogenerated electrons. Thus, the h-MFP increases drastically if the holes leave the electron-rich illuminated area, drifting towards the extracting contact. Due to the shorter e-MFP, the photoresponse ascribed to mechanism 1 is restricted to the region close to the positive (electron-extracting) electrode.

Mechanism 2 (photoconductance) leads to a conductance enhancement at all positions illuminated throughout the channel. However, hole injection and space-charge-limited current are well-known bottlenecks which are also localized at the positive electrode [18]. Additionally, a high density of photogenerated electrons near the positive contact may lead to a reduced injection barrier for holes. Therefore, mechanism 2 also results in a photoresponse enhancement at the positive electrode.

To analyze the spatial dependence of the photoresponse quantitatively, line cuts along the TFT channel axis for different gate voltages are presented in Fig. 4. The observed

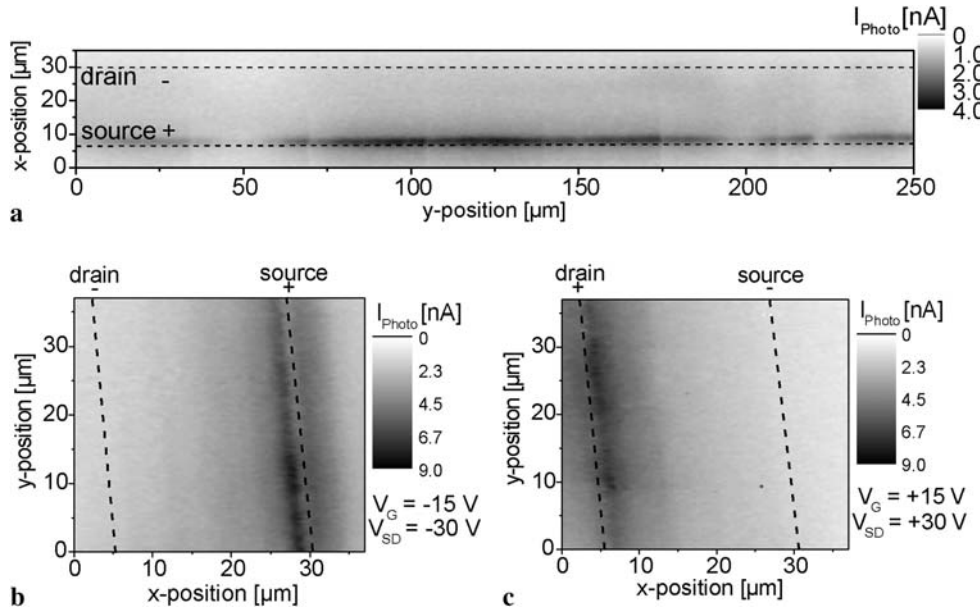


**Fig. 3** Photoresponse (nA) in dependence on the  $x$ - $y$  position of the laser spot at the sample. Positions of source and drain contacts, as determined by the optical confocal scan, are indicated. (a) Photoreponse map of a 250- $\mu\text{m}$ -wide channel region for a gate voltage of  $V_G = -10$  V and a source-drain voltage of  $V_{DS} = -5$  V. In order to cover such a wide region, a number of consecutively performed scans

were stitched together. (b) Photoreponse map of a 37.5- $\mu\text{m}$ -wide channel region at a source-drain voltage of  $V_{DS} = -30$  V and a gate-source voltage of  $V_G = -15$  V. (c) Photoreponse map of the same channel region as in (b) for a source-drain voltage of  $V_{DS} = +30$  V and a gate-source voltage of  $V_G = +15$  V (see footnote 1)

photoreponse scales with the gate field (see inset of Fig. 4). In the following, we perform 3D drift-diffusion simulations<sup>2</sup> extended by photogeneration and bimolecular recombination [see (1) and (2)] to describe the experimental data.

In the simulations we use a value of  $E_g = 1.95$  eV for the pentacene transport band gap [13] and a hole barrier of 0.45 eV at the gold contacts. A hole mobility of  $\mu_h = 8 \times 10^{-2}$  cm $^2$  V $^{-1}$  s $^{-1}$  has been obtained by fitting of the output and transfer characteristics of the device (compare Fig. 2).

Simulation results for the photoreponse as a function of the laser position along the channel are compared in Fig. 4.  $\eta$ ,  $r$ , and the electron mobility  $\mu_e$  have been varied to fit the data, while the hole mobility  $\mu_h$  has been kept at its nominal value. The simulation reproduces the measurements. Good agreement is obtained for the parameter set of  $\eta = 0.1$ ,  $r = 10^{-16}$  cm $^3$  s $^{-1}$ , and  $\mu_e = 10^{-3}$  cm $^2$  V $^{-1}$  s $^{-1}$ .

In order to verify which of the two mechanisms (photocurrent/photoconductance) dominates the photoreponse signal, we analyzed the simulation results in more detail. Using the fitting parameters of the drift-diffusion simulations we have extracted the potential profile and the light-induced electron density for two different laser positions from the simulation (see Fig. 5). For the laser spot close to the positive source, the photogenerated electron current reaches into

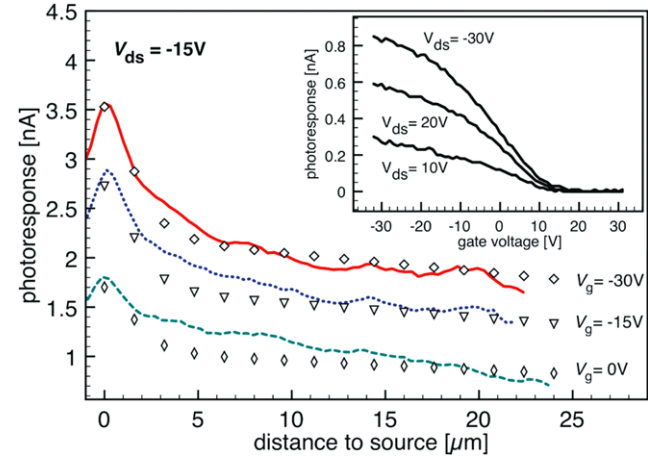


**Fig. 4** Photoreponse in dependence on the distance to the source contact of the OTFT for a source-drain voltage of  $V_{DS} = -15$  V and various gate voltages. Solid lines represent measured data, whereas symbols show the results of drift-diffusion simulations. The inset shows the photoreponse in dependence on the gate voltage for different source-drain voltages if the laser spot remains focused within the channel close to the source contact

the contact (see Fig. 5) and mechanism 1 (photocurrent) is effective. Further inspection reveals that the potential drop across the source contact is also significantly reduced for a laser position close to the source. For positions far away from the source, the electron current decays almost entirely before it reaches the electrode. In this region the photore-

<sup>2</sup>We use a modified version of the commercially available tool ISE-TCAD, Synopsis Inc. ([www.synopsis.com](http://www.synopsis.com)).

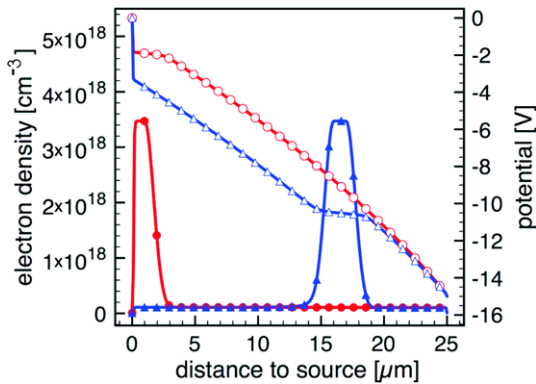


**Fig. 5** Simulated potential profiles (open symbols) and electron densities (filled symbols) for laser positions close to the source (circles) and far away from the source (triangles) ( $V_{DS} = -15$  V,  $V_G = -30$  V)

sponse is dominated by conductance enhancement due to mechanism 2 (photoconductance). Here, the illumination results in a flat (i.e. short-circuited) potential region, originating from the large photogenerated charge-carrier densities.

## 5 Summary

In summary, pentacene OTFTs have been fabricated and analyzed by spatially resolved photoresponse measurements using a lock-in technique. First, the technique allows for the visualization of contact deficiencies. We assign this to the varying quality of the pentacene film near the contacts. Second, photoresponse maps show a strong enhancement of the photoresponse towards the positively biased electrode. In order to explain this behavior, we have established a generation–recombination model resulting in a photoresponse which matches our experimental data. Depending on the position of illumination, the photoresponse signal is dominated by different mechanisms. For illumination close to the positive contact, the photoresponse is a result mainly due to photocurrent and due to hole-injection-barrier lowering. For laser positions further apart from the positive contact, local conductance enhancement in the channel governs the photoresponse signal.

**Acknowledgements** We thank J. Pflaum, Universität Würzburg, for pentacene purification and J.P. Kotthaus for providing the laboratory for these experiments. We also gratefully acknowledge financial support from the Deutsche Forschungsgemeinschaft (DFG Ni 632/2-1) within SPP 1121, the Center for NanoScience (CeNS), and the Nanosystems Initiative Munich (NIM). Discussions with U. Beierlein and help from M. Huth are gratefully acknowledged.

## References

1. C.D. Dimitrakopoulos, P.R.L. Malenfant, *Adv. Mater.* **14**, 99 (2002)
2. G. Horowitz, *Adv. Mater.* **10**, 365 (1998)
3. Y.M. Sun, Y.Q. Liu, D. Zhu, *J. Mater. Chem.* **15**, 53 (2005)
4. I. Yagi, K. Tsukagoshi, Y. Aoyagi, *Appl. Phys. Lett.* **84**, 813 (2004)
5. P.V. Pesavento, R.J. Chesterfield, C.R. Newman, C.D. Frisbie, *J. Appl. Phys.* **96**, 312 (2004)
6. H. Klauk, G. Schmid, W. Radlik, W. Weber, L. Zhou, C.D. Sheraw, J.A. Nichols, T.N. Jackson, *Solid-State Electron.* **47**, 297 (2003)
7. P.V. Necliudov, M.S. Shur, D.J. Gundlach, T.N. Jackson, *Solid-State Electron.* **47**, 259 (2003)
8. I. Kymmissis, C.D. Dimitrakopoulos, S. Purushothaman, *IEEE Trans. Electron Devices* **48**, 1060 (2001)
9. T. Muck, J. Fritz, V. Wagner, *Appl. Phys. Lett.* **86**, 232101 (2005)
10. N. Yoneya, M. Noda, N. Hirai, K. Nomoto, M. Wada, J. Kasahara, *Appl. Phys. Lett.* **85**, 4663 (2004)
11. T. Agostinelli, M. Caironi, D. Natali, M. Sampietro, P. Biagioni, M. Finazzi, L. Duo, *J. Appl. Phys.* **101**, 114504 (2007)
12. A. Maliakal, K. Raghavachari, H. Katz, E. Chandross, T. Siegrist, *Chem. Mater.* **16**, 4980 (2004)
13. J. Lee, S.S. Kim, K. Kim, J.H. Kim, S. Im, *Appl. Phys. Lett.* **84**, 1701 (2004)
14. C. Meyer, O. Sqalli, H. Lorenz, K. Karrai, *Rev. Sci. Instrum.* **76**, 063706 (2005)
15. R. Ruiz, A.C. Mayer, G.G. Malliaras, B. Nickel, G. Scoles, A. Kazimirov, H. Kim, R.L. Headrick, Z. Islam, *Appl. Phys. Lett.* **85**, 4926 (2004)
16. A. Di Carlo, F. Piacenza, A. Bolognesi, B. Stadlober, H. Maresch, *Appl. Phys. Lett.* **86**, 263501 (2005)
17. O. Mitrofanov, D.V. Lang, C. Kloc, J.M. Wikberg, T. Siegrist, W.-Y. So, M.A. Sergent, A.P. Ramirez, *Phys. Rev. Lett.* **97**, 166601 (2006)
18. D.J. Gundlach, L. Zhou, J.A. Nichols, T.N. Jackson, P.V. Necliudov, M.S. Shur, *J. Appl. Phys.* **100**, 024509 (2006)